Metrol. Meas. Syst., Vol. 27 (2020) No. 3, pp. 417–425
DOI: 10.24425/mms.2020.134588

METROLOGY AND MEASUREMENT SYSTEMS
Index 330930, ISSN 0860-8229
www.metrology.wat.edu.pl

IMPEDANCE SPECTROSCOPY IN H_2 SENSING WITH TiO_2 / SnO_2 NANOMATERIALS

Bartłomiej Szafraniak[1)], Anna Kusior[2)], Marta Radecka[2)], Katarzyna Zakrzewska[1)]

1) *AGH University of Science and Technology, Faculty of Computer Science, Electronics and Telecommunications, al. A. Mickiewicza 30, 30-059 Kraków, Poland* (*szafrani@agh.edu.pl, zak@agh.edu.pl*)
2) *AGH University of Science and Technology, Faculty of Materials Science and Ceramics, al. A. Mickiewicza 30, 30-059 Kraków, Poland* (✉ *akusior@agh.edu.pl,* +48 12 617 24 68, *radecka@agh.edu.pl*)

Abstract

Alternating current a.c. measurements enable to understand the physical and chemical processes occurring in semiconductor materials. Impedance spectroscopy has been successfully applied to study the responses of gas sensors based on metal oxides, such as TiO_2, SnO_2 and TiO_2/SnO_2 nanocomposites. This work is devoted to dynamic measurements of hydrogen sensor behaviour over the temperature range of 300–450°C. Frequency dependence of the impedance signal gives evidence that 50 mol% TiO_2/50 mol% SnO_2 nanocomposites should be treated as resistive-type sensors. Temporal evolution of the response to 500 ppm H_2 at 320°C indicates a very short response time and much longer recovery.

Keywords: impedance spectroscopy, TiO_2, SnO_2, hydrogen detection, resistive-type gas sensors.

1. Introduction

Alternating current a.c. impedance spectroscopy is a form of analysis that is widely used to study the electrical behaviour of polycrystalline ceramic materials [1]. Frequency dependence of the measured signal usually allows us to distinguish between the bulk, grain boundary, and electrode contributions to the overall impedance [2–4]. However, in the case of metal oxide n-type nanomaterials where the grains are fully depleted of electrons, bulk and grain boundary effects merge [5].

Impedance spectroscopy can be successfully applied to dynamic measurements of the responses of gas sensing materials [6, 7]. A.c. mode of operation presents many advantages over the classical d.c. electrical signals usually employed for gas sensing [1] such as:

– elimination of polarization effects in constant fields,
– inherent strategy for selectivity improvement,
– possibility to separate contributions of the interfaces from the bulk.

The main advantage, usually not fully recognized, is that impedance spectroscopy allows us to state whether we deal with the resistive-type or capacitance sensor and to establish whether both effects are mixed. This aspect of the impedance spectroscopy constitutes the motivation for this work.

On the other hand, due to the nature of a.c. measurement, when scanning over a wide frequency range it might be impossible to follow fast changes in the electric signal upon admission of the detected gas. Therefore, the studies of kinetics of gas-solid interactions require narrowing the range of frequencies in order to eliminate its lowest part (10^{-3}–1 Hz).

This work focuses on the studies of gas sensing responses to hydrogen of TiO_2/SnO_2 nanomaterials by impedance spectroscopy. The aim is to prove that the sensors prepared are really the resistive-type ones. This is usually claimed for metal-oxide semiconductors while such a conclusion cannot be drawn from d.c. measurements.

Both TiO_2 and SnO_2 play an important role in the field of gas sensing [5, 8-13]. Our previous publications [5, 8, 11, 14] concentrated on a TiO_2-SnO_2 system in the form of thin films, nanocomposites, solid-solutions, *etc.* A profound structural analogy between the constituents, *i.e.*, tin dioxide and titanium dioxide, makes this system particularly promising for many applications [8–11, 15]. The influence of its chemical composition on the electrical properties has also been shown [8–18]. However, here for the first time, the response and recovery signals upon exchange of H_2/air atmosphere are demonstrated based on temporal analysis of impedance spectra.

2. Experiment

Nanocomposites of 50 mol% TiO_2/50 mol% SnO_2 were obtained as described in detail in [11] starting from commercial (Sigma Aldrich) nanopowders of titanium dioxide and tin dioxide. A planetary mill (Fritsch, Pulverisette 6) with zirconia balls was used for mechanical grounding of nanopowders submerged in ethanol. For gas sensing measurements, 7 mm in diameter and 1 mm thick tablets were assembled from nanopowders mixed with polyethylene glycol. Prior to calcination at 450°C, the tablets were subject to isostatic pressing at 25 MPa. Contact Pt electrodes were applied for the electrical measurements.

Data concerning the composition and microstructure are collected in Table 1 as described in detail previously [8, 14]. Starting nanopowders from which 50 mol% TiO_2/50 mol% SnO_2 nanocomposites were prepared differ from each other in crystallite d_{XRD} and grain size D_{SEM}, d_{XRD} = 28 nm, D_{SEM} = 83−133 nm for SnO_2 and d_{XRD} = 8 nm, D_{SEM} = 30−33 nm for TiO_2 which is reflected in the resulting nanocomposite. Density of both constituents is smaller than usually encountered [19] which is the consequence of significant porosity of 48–62%.

Table 1. Chemical composition, crystallite size, d_{XRD}, specific surface area, SSA, average pore size, porosity and density, grain size D_{SEM} for TiO_2/SnO_2 nanocomposites in the form of powders and tablets, where *C* – cassiterite, *R*– rutile, *BJH* – the Barrett-Joyner-Halenda method of pore size distribution determination.

Chemical composition	**Powders**			**Tablets**			
	d_{XRD} (nm) [8]		SSA (m^2/g) [8]	Pore size from *BJH* (nm) [14]	Porosity (%)[14]	Density (g/cm^3) [14]	D_{SEM} (nm)
	TiO_2	SnO_2					
SnO_2 (*C*)		28	21.2	28.7	48.0	3.61	83–133
50 mol% TiO_2/ 50 mol% SnO_2 (*R*/*C*)	8	28	64.5	16.6	53.2	2.62	33–83
TiO_2 (*R*)	8		158.5	11.9	61.4	1.63	30–33

Metrol. Meas. Syst., Vol. 27 (2020), No. 3, pp. 417–425
DOI: 10.24425/mms.2020.134588

Impedance spectra were acquired by means of a Solartron 1296 dielectric interface and a Solartron 1260 dielectric response frequency analyser. The maximum frequency range of 10^{-3}–10^{6} Hz was explored. The a.c. signal amplitude was set to 10 mV. Electrical measurements were performed at different but constant temperatures selected within the range of 300–450°C. Synthetic air was used as a reference gas for hydrogen detection. Gas atmosphere was controlled with two separate mass flowmeters, one in the line of synthetic air, one in Ar+H_2 line.

Analysis of the recorded impedance spectra was performed with the ZView software. In order to determine the contribution of ohmic resistance R and that of capacitance C, two different equivalent circuits were proposed as explained later in the text. In both models used for fitting the experimental spectra, the basic unit of the circuit consisted of a resistor R in parallel with a constant phase element CPE. The CPE is an element of impedance Z_{CPE} defined as:

$$Z_{CPE} = A^{-1}(j\omega)^{-n} \tag{1}$$

where: A and n are constant coefficients, j represents an imaginary unit, ω is an angular frequency. The coefficient n being different from 1, gives information about the deviation from capacitive behaviour.

3. Results and discussion

Electrical properties of material in which grain (bulk and boundary) and electrode effects play an important role were determined using impedance spectroscopy over a wide frequency range from 10^{-3} to 10^{6} Hz. Figure 1 shows two types of graphic representations of impedance data. The absolute value of the impedance $|Z|$ vs. frequency (a Bode plot) is presented in Fig. 1a.

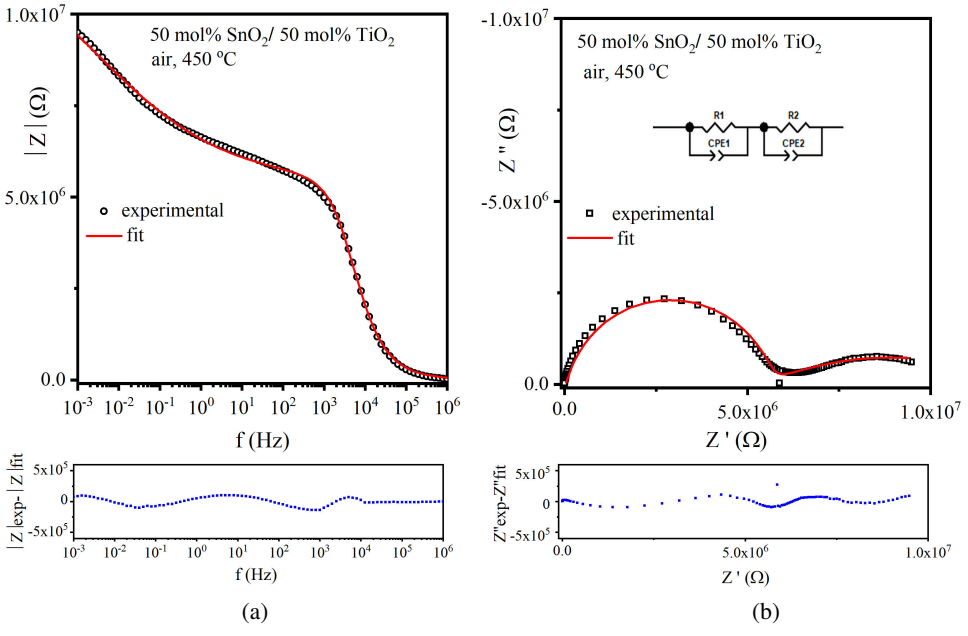

Fig. 1. Impedance plots for 50 mol% TiO_2/50 mol% SnO_2 nanocomposite illustrating the principle of measurement over a very wide frequency range. a) Bode representation; b) Nyquist representation. Parameters of the electrical equivalent circuit are $R_1 = (5.417 \pm 0.054) \cdot 10^6$ ohm, $A_1 = (2.655 \pm 0.192) \cdot 10^{-11}$ $F^{0.88}$, $n_1 = 0.88 \pm 0.01$, $R_2 = (6.973 \pm 0.447) \cdot 10^6$ ohm, $A_2 = (4.176 \pm 0.132) \cdot 10^{-7}$ $F^{0.26}$, $n_2 = 0.26 \pm 0.01$.

A Nyquist representation shows the imaginary Z' part as a function of the real Z'' part (Fig. 1b). Such a wide frequency range is necessary in order to create a suitable model of the electric circuit. In the case of ideal behaviour of a polycrystalline material, the complex plane plot (the Nyquist representation) contains a succession of semicircles related to the bulk material, grain boundary and electrode phenomena. In general, the separate semicircles for bulk and grain boundary can be seen in the Nyquist plots if the processes occurring in the materials are characterized by very different, *i.e.*, more than two orders of magnitude, relaxation times [1, 2].

However, as shown in Fig. 1b, for TiO_2-SnO_2 nanocomposites of particular composition 50 mol%/50 mol% the Nyquist plot consists of a well-developed high frequency semicircle representing material properties followed by a deformed semicircle at lower frequencies corresponding to the electrode contribution. Bulk and grain boundary processes cannot be distinguished.

An equivalent circuit consisting of two resistance-*CPE* elements in series was used for fitting the IS spectra. The values of parameters of the circuit indicate that a polarizing process takes place at high frequencies (n_1 high, almost equal to 1 gives evidence of capacitive behaviour) while diffusive processes dominate over the low frequency range (n_2 small). Distribution of the absolute fit error is included in Fig. 1 below the Bode and Nyquist plots.

In this work, possibly due to the nanocrystalline nature of the composite material composed of 50 mol% SnO_2/50 mol% TiO_2, the IS spectrum within the range of frequencies extending from 1 to 10^6 Hz consists of one well-developed high frequency semicircle which is responsible for bulk/surface processes as seen in Fig. 2a. Moreover, the IS spectra of the constituents of the

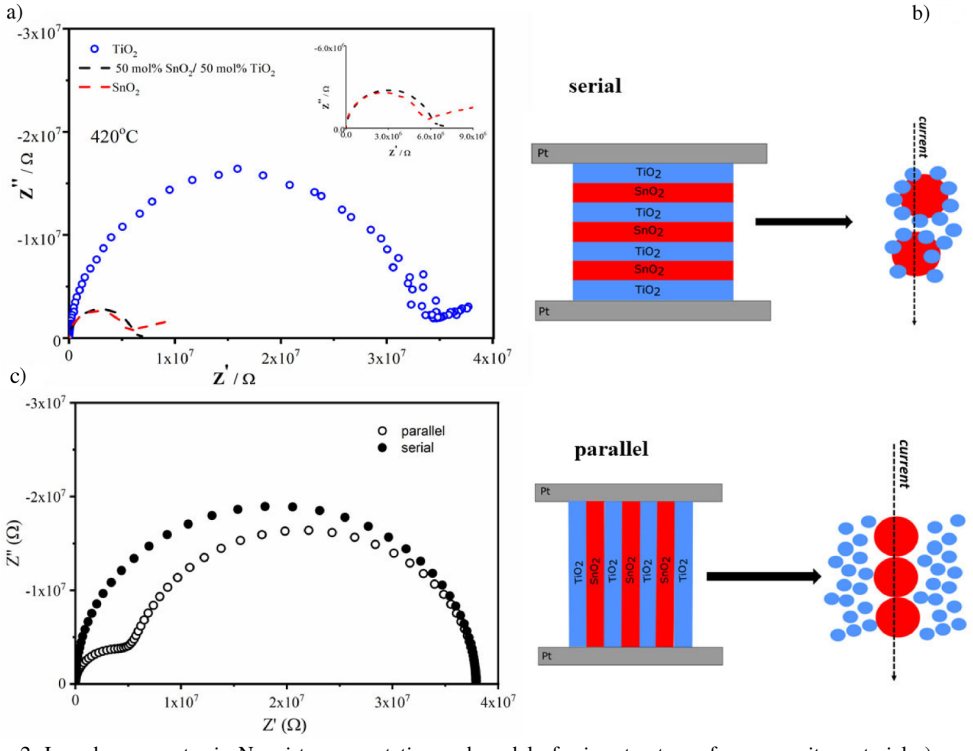

Fig. 2. Impedance spectra in Nyquist representation and model of microstructure of a composite material a) experimental impedance spectra for TiO_2, SnO_2 and 50 mol% TiO_2/50 mol% SnO_2 nanocomposite; b) models of composite microstructure described by series and parallel connections; c) theoretical simulation of impedance spectra for 50 mol% TiO_2/50 mol% SnO_2 nanocomposite with different microstructures.

Metrol. Meas. Syst., Vol. 27 (2020), No. 3, pp. 417–425
DOI: 10.24425/mms.2020.134588

nanocomposite, *i.e.*, TiO_2 and SnO_2 are included in Fig. 2a. Over the low frequency range, a part of the deformed semicircle is visible. No separation of bulk and grain boundary processes is observed.

An analysis of the experimental data indicates that TiO_2 has higher electrical resistance than SnO_2. The bulk/surface electrical resistances are: $3.25 \cdot 10^7$ Ω, $5.41 \cdot 10^6$ Ω, $6.15 \cdot 10^6$ Ω for TiO_2, SnO_2 and 50 mol% SnO_2/50 mol% TiO_2 nanocomposite, respectively. The time constants of the composite components differ by two orders of magnitude ($\tau(TiO_2) = 1.63 \cdot 10^{-3}$ s and $\tau(SnO_2) = 4.19 \cdot 10^{-5}$ s) which should manifest itself as resolved semicircles in the Nyquist plot. However, in fact even in this case the separation did not occur. Therefore, theoretical modelling has been performed based on IS data concerning TiO_2 and SnO_2. Two equivalent circuit models representing composites with microstructure described by series and parallel connections (Fig. 2b) were used for simulation of the impedance spectra. Fig. 2c demonstrates the results of a simulation of $Z'' = f(Z')$ for 50 mol% SnO_2/50 mol% TiO_2 nanocomposite. A separation of semicircles takes place in the case of parallel connection, however, this type of morphology does not seem possible for nanocomposites in question. The serial connection, which is more probable, reveals only one single arc in the Nyquist representation.

Figure 3 demonstrates dynamic evolution of impedance spectra in the Nyquist representation over the limited frequency range extending from 1 Hz to 10^6 Hz upon admission (Fig. 3a) and removal of hydrogen (Fig. 3b). The low frequency region was suppressed because it is not representative for gas interaction with the nanocomposite but rather for its interface with the Pt electrode.

Similarly to the dc signals, in the impedance spectra one can observe the influence of hydrogen as a function of time. The response time is very short so the circles are barely distinguished (Fig. 3a). The recovery time is much longer and that is why the circles observed at a certain time intervals are very well separated (Fig. 3b).

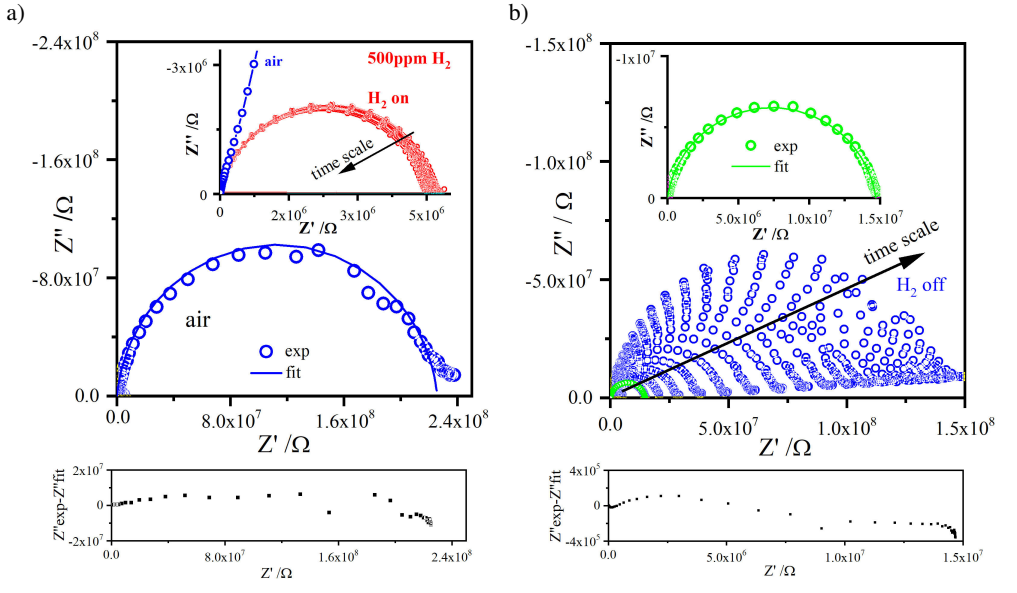

Fig. 3. Dynamic evolution of impedance spectra for 50 mol% TiO_2/50 mol% SnO_2 nanocomposite in a Nyquist representation at the temperature of 320°C upon hydrogen admission (500 ppm) a) response to hydrogen; b) recovery after air purging; the frequency range extends from 1 Hz to 10^6 Hz. Absolute error of the fit $Z''_{exp} - Z''_{fit}$ is shown below the Nyquist plots.

Gas sensing behavior of the nanocomposites can also be analyzed by drawing the impedance module $|Z|$ as a function of frequency f (Fig. 4). As it can be seen, upon interaction with hydrogen the absolute value of the impedance decreases and plateau width increases (Fig. 4a). Figure 4b shows the frequency dependence of the ratio $\frac{|Z_{air}|}{|Z_{H2}|}$ of absolute values of the impedances in air $|Z_{air}|$ and in hydrogen $|Z_{H2}|$. As Fig. 4b reveals, the $\frac{|Z_{air}|}{|Z_{H2}|}$ is the biggest in the low frequency range $f = 1-10$ Hz. At higher frequencies, it decreases to reach a constant level at above 10^3 Hz. Therefore, in order study the gas sensing responses with impedance spectroscopy, an appropriate frequency range should be chosen.

The analysis of a circuit comprising a parallel connection of a resistor R with a capacitor C yields capacitive behaviour at high frequencies and resistive type characteristics at low frequencies. This can be inferred from the general expression for the equivalent impedance of such a circuit [1]:

$$Z = \frac{R - j\omega R^2 C}{1 + \omega^2 R^2 C^2} \,. \tag{2}$$

Charge carriers travelling through a sample have to overcome successive impedances of two different regions: bulk of the grain and the grain boundary that differ in their dielectric properties. The high frequency component usually corresponds to the bulk properties but sometimes the frequencies that allow to observe this effect cannot be achieved due to the limited frequency band of the measuring device [1]. On the contrary, the lower frequency range is where one can study the grain boundary contribution where both capacitance C and resistance R are much larger than those of the bulk of the grain due to the formation of the depletion region. This region is particularly affected by gas adsorption.

Differences in the response and the recovery times are quite visible when one compares the data in Fig. 4a (adsorption of hydrogen) with Fig. 4c (desorption of water).

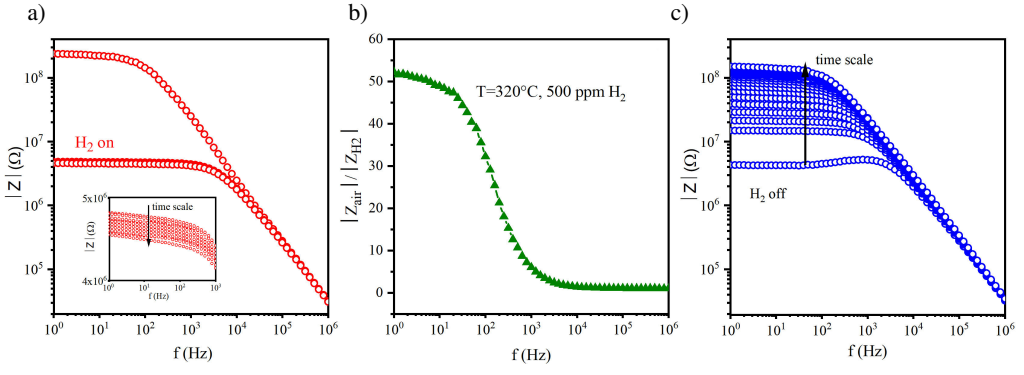

Fig. 4. Dynamic evolution of the impedance spectra for a) 50 mol% TiO_2/50 mol% SnO_2 nanocomposite as a Bode plot at the temperature of 320°C upon hydrogen admission (500 ppm), b) response to hydrogen, c) recovery after air purging; the frequency range extends from 1 Hz to 10^6 Hz.

The mechanism of interaction of hydrogen with SnO_2/TiO_2 nanograins can be described by the following reactions:

$$O_{2ads} + e' \leftrightarrow 2O^-$$

$$O^- + H_2 \leftrightarrow H_2O + e'.$$

Metrol. Meas. Syst., Vol. 27 (2020), No. 3, pp. 417–425
DOI: 10.24425/mms.2020.134588

As shown in our previous work [20] activation energy of H_2 adsorption is smaller than the energy required for H_2O desorption. Water desorption is quite a complicated process as discussed in [13] and, within the temperature range applied in this work, involves its onset (at about 280°C) followed by desorption of OH^- at about 400°C. Moreover, diffusion through the porous microstructure can be responsible for such a very long time of signal recovery.

The equivalent circuit used to analyze the impedance spectra for 50 mol% TiO_2/50 mol% SnO_2 nanocomposite upon hydrogen admission (500 ppm) and recovery after air purging is simplified and composed of one unit only, *i.e.*, a resistor R and a *constant phase element* (CPE) in parallel. The results of the fitting of IS spectra in order to extract R and *CPE* as a function of measurement number are shown in Fig. 5. For all the cases studied, the parameter n of the *CPE* element takes values close to 0.90–0.95 which corresponds to a capacitance. Hsu and Mansfeld [21] gave the following equation for calculating the true capacitance, C_{true} in the case of the depressed semicircle when *CPE* is in parallel with a resistance:

$$C_{\text{true}} = A(\omega_{\max})^{n-1}, \tag{3}$$

where $\omega_{\max}$ represents the frequency at which the imaginary component of $Z'' = f(Z')$ reaches a maximum. As it can be seen, the electrical resistance R reacts to hydrogen presence and withdrawal. The true capacitance C_{true} is not affected by the changes in the composition of atmosphere. From this type of analysis one can draw a conclusion that we deal with the resistive-type gas sensors.

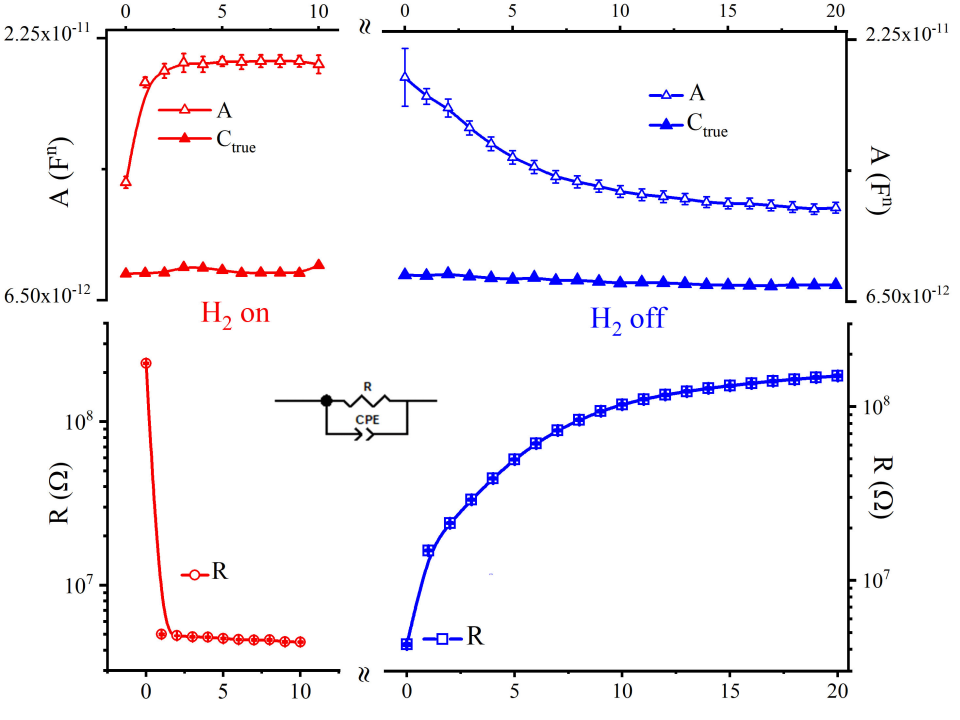

Fig. 5. Dynamic changes of parameters of the equivalent circuit R and C_{true} in consecutive steps of exposure to hydrogen (H_2 on) and air (H_2 off). Error bars are included.

4. Conclusions

The work carried out on gas sensing performance of TiO_2/SnO_2 nanocomposites by means of impedance spectroscopy allowed us to draw the following conclusions:

1. Separation between the bulk and grain boundary effects, usually expected in the case of two orders of magnitude difference in the relaxation times, was not observed probably due to specific morphology of nanocomposites resulting in serial connection of elements.
2. Resistive-type behaviour in gas sensing was confirmed by the analysis of the frequency dependence of the impedance responses upon interaction of the nanocomposite semiconductor with hydrogen.
3. Time constants for adsorption and desorption were found to be significantly different which could be attributed to specific morphology of nanocomposites.
4. Impedance spectroscopy provides more information about the processes occurring in the structure than d.c. measurements which, in turn, helps to optimize the sensor characteristics.

Acknowledgements

This work has been financed by the Polish National Center of Science, NCN, grant decision no. 2016/23/B/ST7/00894.

References

[1] Schipani, F., Miller, D.R., Ponce, M.A., Aldao, C.M., Akbar, S.A., Morris, P.A. (2016). Electrical Characterization of Semiconductor Oxide-Based Gas Sensors Using Impedance Spectroscopy: A Review. *Reviews in Advanced Sciences and Engineering*, 5(1), 86–105.

[2] Macdonald, J.R., Barsoukov, E. (2005). Impedance Spectroscopy: Theory, Experiment, and Applications. Hoboken: John Wiley & Sons, Inc.

[3] Aguir, K., Labidi, A., Lambert-Mauriat, C. (2006). Impedance spectroscopy to identify the conduction mechanisms in WO_3 sensors. *Sensors*, 267–270.

[4] Lacz, A., Grzesik, K., Pasierb, P. (2019). Electrical properties of $BaCeO_3$-based composite protonic conductors. *Journal of Power Sources*, 279, 80–87

[5] Lyson-Sypien, B., Kusior, A., Rekas, M., Zukrowski, J., Gajewska, M., Michalow-Mauke, K., Graule, T., Radecka, M., Zakrzewska, K. (2017). Nanocrystalline TiO_2/SnO_2 heterostructures for gas sensing. *Beilstein J. Nanotechnology*, 8, 108–122.

[6] Al-Hardan, Naif H., Aziz, A.A., Abdullah, M.J., Ahmed, N.M. (2018). Conductometric Gas Sensing Based on ZnO Thin Films: An Impedance Spectroscopy Study. *ECS Journal of Solid State Science and Technology*, 7(9), 487–490.

[7] Shahkhatunia, G.H., Aroutiouniana, V.M., Arakelyana, V.M., Aleksanyana, M.S., Shahnazaryana, G.E. (2019). Investigation of Sensor Made of ZnO:La for Detection of Hydrogen Peroxide Vapours by Impedance Spectroscopy Method. *Journal of Contemporary Physics*, 54(2), 188–195.

[8] Radecka, M., Kusior, A., Lacz, A., Trenczek-Zajac, A., Lyson-Sypien, B., Zakrzewska, K. (2012). Nanocrystalline TiO_2/SnO_2 for gas sensors. *Journal of Thermal Analysis and Calorimetry*, 108(3), 1079–1084.

[9] Zeng, W., Liu, T., Wang, Z. (2010). Sensitivity improvement of TiO_2 – doped SnO_2 to volatile organic compounds. *Physica E: Low-dimensional Systems and Nanostructures*, 43(2), 633–638.

Metrol. Meas. Syst., Vol. 27 (2020), No. 3, pp. 417–425
DOI: 10.24425/mms.2020.134588

[10] Carotta, M.C., Gherardi, S., Guidi, V., Malagù, C., Martinelli, G., Vendemiati, B., Sacerdoti, M., Ghiotti, G., Morandi, S. (2009). Electrical and spectroscopic properties of $Ti_{0.2}Sn_{0.8}O_2$ solid solution for gas sensing. *Thin Solid Films*, 517(22), 6176–6183.

[11] Radecka, M., Zakrzewska, K., Rekas, M. (1998). SnO_2–TiO_2 solid solutions for gas sensors. *Sensors and Actuators B: Chemical*, 47(1-3), 193–199.

[12] Gwiżdż, P., Brudnik, A., Zakrzewska, K. (2015). Hydrogen Detection With a Gas Sensor Array – Processing and Recognition of Dynamic Responses Using Neural Networks. *Metrology and Measurement Systems*, 22(1), 3–12.

[13] Suchorska-Woźniak, P., Rac, O., Fiedot, M., Teterycz, H. (2016). The Impact of Sepiolite on Sensor Parameters during the Detection of Low Concentrations of Alcohols. *Sensors*, 16(11), 1881.

[14] Kusior, A., Radecka, M., Zych, Ł., Zakrzewska, K., Reszka, A., Kowalski, B.J. (2013). Sensitization of TiO_2/SnO_2 nanocomposites for gas detection. *Sensors and Actuators B: Chemical*, 189, 251–259.

[15] Carney, C.M., Yoo, S., Akbar, S.A. (2005). TiO_2-SnO_2 nanostructures and their H_2 sensing behavior. *Sensors and Actuators B: Chemical*, 108, 29–33.

[16] Van Duy, N., Van Hieu, N., Huy, P.T., Chien, N.D., Thamilselvan, M., Yi, J. (2008). Mixed SnO_2/TiO_2 included with carbon nanotubes for gas-sensing application. *Physica E: Low-dimensional Systems and Nanostructures*, 41(2), 258–263.

[17] Hübner, M., Pavelko, R., Kemmler, J., Barsan, N., Weimar, U. (2009). Influence of material properties on hydrogen sensing for SnO_2 nanomaterials. *Procedia Chemistry*, 1(1), 1423–1426.

[18] Yamazoe, N. (2005). Toward innovations of gas sensor technology. *Sensors and Actuators B: Chemical*, 108(1-2), 2–14.

[19] Lide, D.R. (2004). *CRC Handbook of Chemistry and Physics*. 85, CRC press.

[20] Lyson-Sypien, B., Radecka, M., Rekas, M., Swierczek, K., Michalow-Mauke, K., Graule, T., Zakrzewska, K. (2015). Grain-size-dependent gas-sensing properties of TiO_2 nanomaterials. *Sensors and Actuators B: Chemical*, 211, 67–76.

[21] Hsu, C.S., Mansfeld, F. (2001). Concerning the Conversion of the Constant Phase Element Parameter Y0 into a Capacitance. *Corrosion*, 57(9), 747–748.